

# Remote sensing of heart rate using millimeter-wave interferometry and probabilistic interpolation

Ilya V. Mikhelson<sup>a</sup>, Sasan Bakhtiari<sup>b</sup>, Thomas W. Elmer II<sup>b</sup>, Shaolin Liao<sup>b</sup>, Alan V. Sahakian<sup>\*a</sup>

<sup>a</sup>Electrical Engineering and Computer Science, Northwestern University, Evanston, IL 60208, USA;

<sup>b</sup>Nuclear Engineering Division, Argonne National Laboratory, Argonne, IL 60439 USA

## ABSTRACT

Using a 94-GHz homodyne interferometer employing a highly-directional quasi-optical lens antenna aimed at a human subject's chest, we can measure chest wall displacement from up to 10m away and through common clothing. Within the chest displacement signal are motions due to cardiac activity, respiration, and gross body movement. Our goal is to find the heart rate of the subject being monitored, which implies isolation of the minute movements due to cardiac activity from the much larger movements due to respiration and body movement. To accomplish this, we first find a subset of the true heartbeat temporal locations (called "confident" heartbeats) in the displacement signal using a multi-resolution wavelet approach, utilizing Symlet wavelets. Although the chest displacement due to cardiac activity is orders of magnitude smaller than that due to respiration and body movement, wavelets find those heartbeat locations due to several useful properties, such as shape matching, high-pass filtering, and vanishing moments. Using the assumption that the "confident" heartbeats are randomly selected from the set of all heartbeats, we are able to find the maximum a posteriori statistics of an inverse Gaussian probability distribution modeling the inter-heartbeat times. We then analyze the "confident" heartbeats and decide which heartbeats are probabilistically correct and which are not, based on the inverse Gaussian distribution we calculated earlier. The union of the "confident" set, after pruning, and the interpolated set forms a very close approximation to the true heartbeat temporal location set, and thus allows us to accurately calculate a heart rate.

**Keywords:** Remote Sensing, Millimeter-Wave, Heartbeat Detection, Heart Rate, Ambulatory Monitoring.

## 1. INTRODUCTION

Gathering remote data on cardiac activity is an important and markedly difficult problem. Examples of applications include medical monitoring (e.g. sleep apnea<sup>1</sup>), security (e.g. malicious intent detection,<sup>2</sup> lying detection<sup>3</sup>), military (e.g. finding hostiles in barricaded buildings<sup>4</sup>), and emergency response (e.g. finding people trapped in a building collapse,<sup>4</sup> triage for burn victims). However, even with a large amount of research, the problem remains difficult due to the plethora of confounding variables and variations of individual humans.

There have been many proposed modalities to find heart rate at a distance, such as using the infrared spectrum,<sup>5</sup> speckle pattern analysis,<sup>6</sup> optical (video) analysis,<sup>7</sup> and electromagnetic waves.<sup>3,4,8-12</sup> Each method has its own advantages and disadvantages. We choose to use electromagnetic waves, specifically millimeter-waves, because of the combination of advantages this provides: a compact transceiver, good range, lighting-independence, and the ability to penetrate through various materials. Specifically, our system finds the displacement of an object (in this case, the chest wall) using the reflected millimeter-wave signal from the surface of the object.

This method dates back to the 1970s and 1980s, when Lin showed that the respiratory and cardiac rates could be gathered from a stationary, clothed subject at a distance of roughly 0.3 m.<sup>8</sup> These early studies used the Doppler effect to calculate the displacements of the chest. Since the radio frequency waves undergo a frequency shift upon reflection from a moving surface (in this case the chest), the change in frequency between

---

\*sahakian@eecs.northwestern.edu; telephone: 1 847 491 3641; fax: 1 847 491 4455; website: <http://users.eecs.northwestern.edu/~sahakian/>

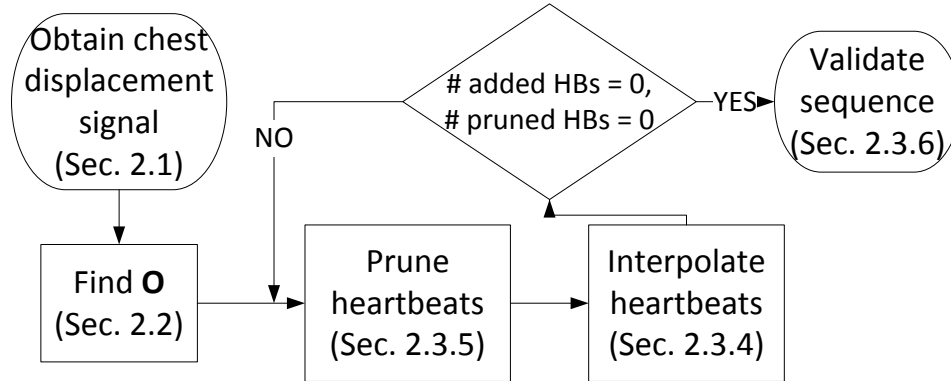


Figure 1: Flowchart of the processing steps for remote detection of cardiac activity.

the transmitted and reflected signals can be analyzed to find the velocity of the chest wall, and subsequently the heart rate and respiratory rate.

A more accurate method was developed, and has gained wide popularity, which uses in-phase and quadrature reflections from the subject's chest in order to find the phase of the reflected signal.<sup>9–13</sup> Since displacement modulates the phase, the movement of the chest can be found directly from the two signals after phase demodulation. The differences in the various approaches have to do with the method to extract the tiny motions due to cardiac activity from the entire chest displacement signal.

This problem is a very difficult one, since motions of the chest due to cardiac activity are eclipsed by most other motions. In fact, most studies have the subject sit still against a back support to minimize the motions due to involuntary swaying back and forth, which is enough to mask the motions due to the heart beating. The only way to physically isolate the motions of interest is to have the subject sit still against a solid back support and to hold his breath. This, however, is a very contrived situation, and although it is good for early-stage proof-of-concept, it fails to address the larger picture of natural monitoring scenarios.

Our work expands the methods we developed previously<sup>14</sup> to further perform a statistical analysis of the detected heartbeats using a wavelet approach. In previous research,<sup>12,14–16</sup> wavelets have been used to decompose the displacement signal. Wavelets provide excellent temporal resolution for rapid events in time, such as heartbeats, and good frequency resolution for slower events in time, such as breathing.<sup>17</sup> However, wavelets alone cannot always find every heartbeat. The focus of our proposed method is on the processing that occurs after a set of heartbeats is detected in the chest displacement waveform. These heartbeats may be erroneous in several locations, so it is important to use the statistics of the detected locations to get the best possible estimate of the true heartbeat locations.

## 2. METHODS

In order to find a subject's cardiac pattern remotely, several steps have to be taken. Fig. 1 provides a summary of the processing steps that will be presented in this section.

### 2.1 Data Acquisition

To find heart rate, we first gather a chest displacement signal, i.e., the movement of the chest perpendicular to the frontal plane. To obtain a chest displacement signal, we use a 94-GHz continuous-wave millimeter-wave interferometer<sup>2</sup> and a National Instruments USB-9239 24-bit analog-to-digital converter with a sampling rate of 5000 Hz to collect in-phase ( $I$ ) and quadrature ( $Q$ ) components of the reflected signal. Details of the system can be found in our previous work.<sup>12</sup> All processing was performed in MATLAB.<sup>18</sup>

The reflected millimeter-wave signal, when the sensor is aimed at the chest, is a combination of several vector components.<sup>9,12</sup> These components also include reflections from stationary or moving objects not related to the

subject. The vector component due to chest wall motion can be isolated using circle-fitting in the in-phase-quadrature ( $I$ - $Q$ ) space. Then, using simplifying assumptions about noise and interference, the measured signal due to chest motion can be used to find the chest displacement signal given by:

$$\text{displacement} = \frac{\lambda_0}{4\pi} \cdot \text{unwrap} \left[ \arctan \left( \frac{Q}{I} \right) \right], \quad (1)$$

where  $\lambda_0 = \frac{2\pi c}{\omega_0}$ ,  $c$  is the speed of light,  $\omega_0 = 94 \cdot 2\pi \cdot 10^9$  rads/s, and “unwrap” denotes phase unwrapping to account for phase discontinuities at  $\pm\pi$ .<sup>12,18</sup>

Using a sampling frequency of 5000 Hz places a limit on the maximum velocity that we can resolve without aliasing. Since one full rotation of the vector in the  $I$ - $Q$  space is caused by a displacement of  $\lambda_0/2$ , the maximum velocity we can resolve ( $v_{\max}$ ) is calculated as:

$$v_{\max} \left( \frac{1}{f_s} \right) = \frac{\lambda_0}{4} \Rightarrow v_{\max} = \frac{f_s \cdot \lambda_0}{4},$$

where  $f_s$  is the sampling frequency. For us, this gives an upper bound of  $v_{\max}=3.987$  m/s (8.724 mph), which amounts to a brisk jog. From empirical data, we have found that the velocity of the chest due to cardiac activity alone, recorded on a seated subject, leaning against a chair back and holding his breath, is not greater than  $\sim 0.01$  m/s. This means that the subject can be moving quite rapidly without aliasing the motions due to cardiac activity.

## 2.2 Initial Heartbeat Temporal Location Detection

Once the displacement signal is generated using eq. (1), individual heartbeat locations must be found. A procedure similar to the one in the work of Mikhelson et al.<sup>12</sup> is used. First, the displacement waveform is downsampled to 50 Hz. Then, the signal is filtered using a Symlet wavelet. The absolute value of this signal is next smoothed with a moving-average filter of varying lengths. The shorter the moving-average filter, the more peaks are preserved in the signal; the longer, the more peaks are smoothed out. We then find the peaks resulting from smoothing with various length filters, and record all their locations, as shown in Fig. 2(a). Finally, a ridge analysis is performed wherein we find the strongest vertical ridges, i.e. the longest vertically-connected components of the graph. The result is also shown in Fig. 2(a). The ridge locations comprise a point process of “confident” heartbeat observations ( $\mathbf{O} = \mathbf{o}_1, \mathbf{o}_2, \dots, \mathbf{o}_N$ ), since these peaks persist across many lengths of moving-average filters, where  $\mathbf{o}_i$  is the time of the  $i$ th “confident” observation.

To evaluate all processing techniques, an electrocardiogram (ECG) was gathered concurrently with the data in order to know where the actual heartbeats ( $\mathbf{S} = \mathbf{s}_1, \mathbf{s}_2, \dots, \mathbf{s}_M$ ) are present, where  $\mathbf{s}_i$  is the time of the  $i$ th true heartbeat. Using the same data as in the previous paragraph, the true heartbeat locations ( $\mathbf{S}$ ), calculated from the ECG, along with the “confident” heartbeats ( $\mathbf{O}$ ), are shown in Fig. 2(b).

## 2.3 Heartbeat Temporal Location Estimation

The locations obtained in Section 2.2 are a good starting point, but an incomplete picture. While those locations are strong candidates to be in the final set of heartbeat locations, they are not guaranteed to be correct, as false positives (FPs) can occur. Additionally, depending on the quality of the reflected signal, there may be many false negatives (FNs) present as well. Since pure interpolation between heartbeats would not actually add any new information, a good model is needed to create a practical and useful algorithm to find the best estimate of  $\mathbf{S}$  based on  $\mathbf{O}$ .

### 2.3.1 Probabilistic Modeling

In order to interpolate missing heartbeats, there has to be a good model of cardiac activity. The probability distribution of the time between subsequent heartbeats has to have the following physiological characteristics: a heartbeat cannot immediately follow another heartbeat due to the refractory period; the probability has a maximum at the subject’s average heart rate at that moment in time; and the probability decreases thereafter.

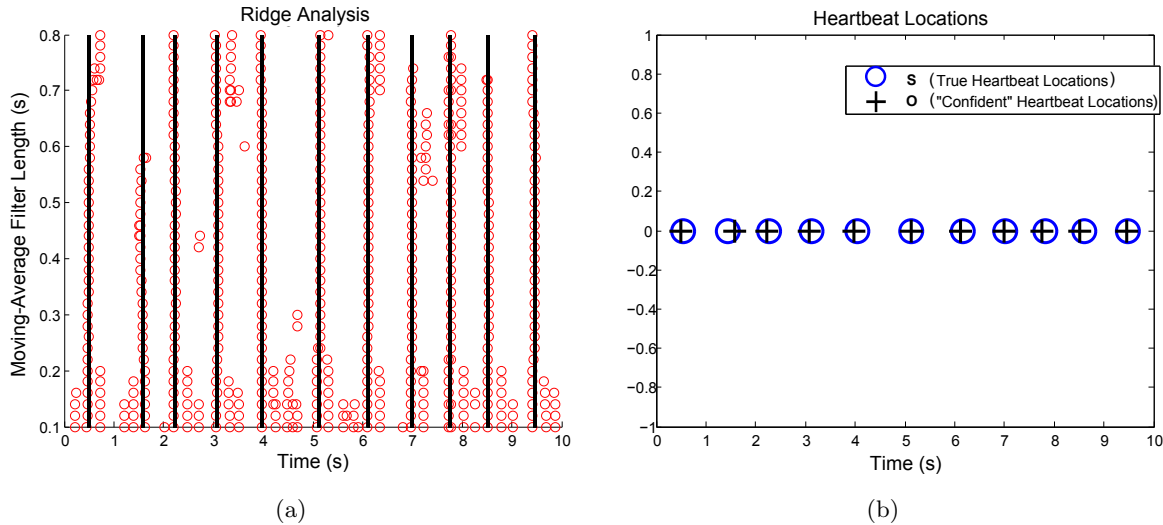


Figure 2: Multiresolution ridge analysis. (a) Peak locations (circles) across various moving-average lengths and strongest ridges (lines) indicating “confident” heartbeat locations. (b) True heartbeat locations and “confident” heartbeat locations.

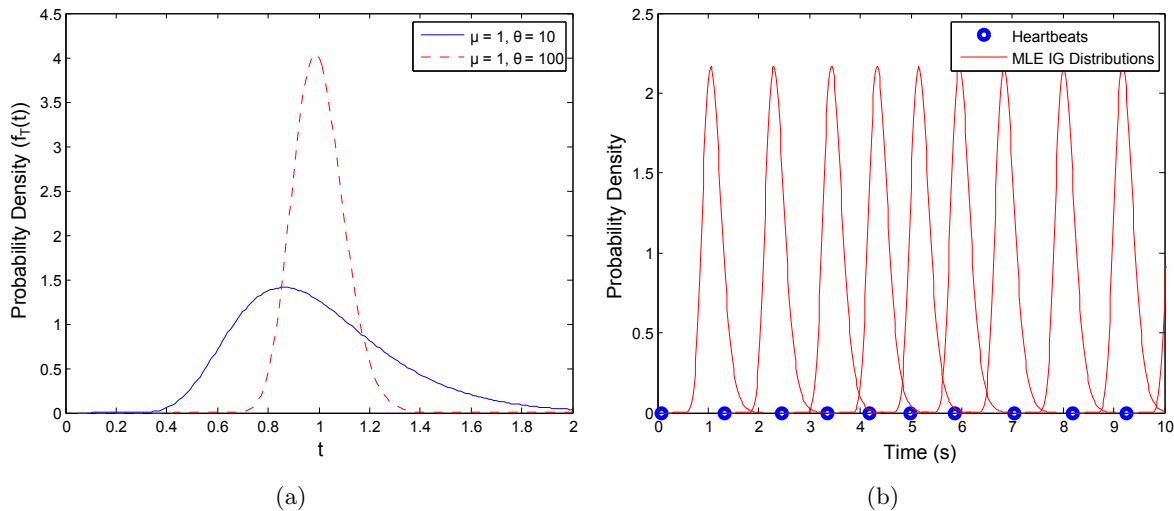


Figure 3: (a) Inverse Gaussian probability density functions, where  $\mu = 1$ , and  $\theta = 10$  and  $\theta = 100$ . (b) Heartbeat locations with superimposed MLE inverse Gaussian distribution originating at each heartbeat.

Such a distribution was found by Barbieri et al.<sup>19</sup> as the inverse Gaussian (*IG*) probability density function (PDF):

$$P[t_i + \tau | t_i; \mu, \theta] = P[\tau | \mu, \theta] \sim IG(\tau; \mu, \theta) = \left( \frac{\theta}{2\pi\tau^3} \right)^{1/2} \exp \left( \frac{-\theta(\tau - \mu)^2}{2\mu^2\tau} \right), \quad (2)$$

where  $\tau$  is the time after a given heartbeat at time  $t_i$ ,  $\mu$  is the average time between heartbeats, and  $\theta$  is a shape parameter that determines the width of the function. An example can be seen in Fig. 3(a). In addition, Fig. 3(b) shows a sequence of heartbeat temporal locations from an ECG with the maximum likelihood estimate (MLE) inverse Gaussian distribution fitted to the inter-heartbeat times superimposed on the sequence. For this sequence,  $\mu = 1.026$  s, and  $\theta = 29.514$  s.

Using the *IG* distribution allows us to better define the heartbeat sequence  $\mathbf{S} = \mathbf{s}_1, \mathbf{s}_2, \dots, \mathbf{s}_M$ . Let

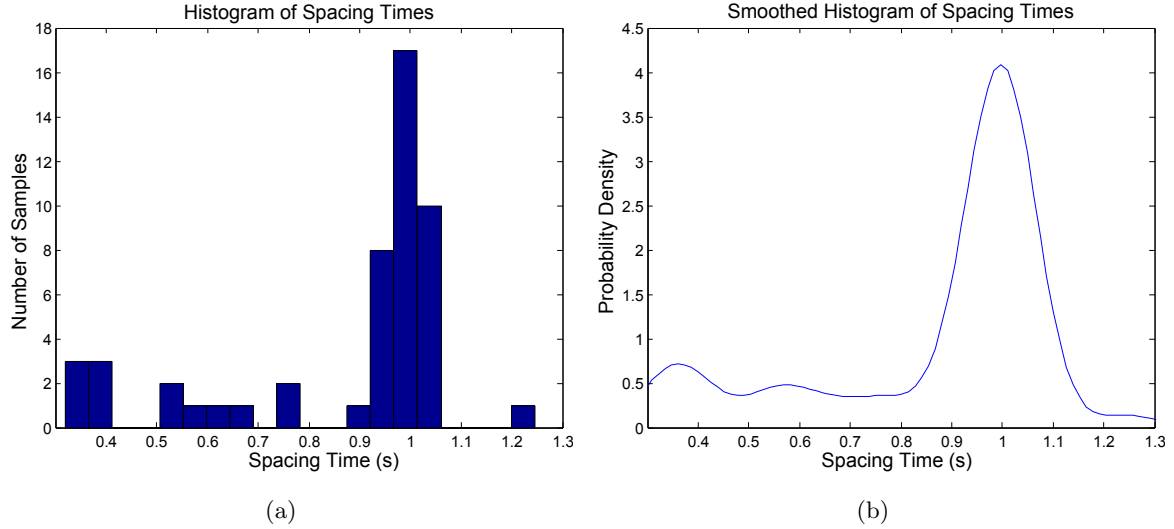


Figure 4: (a) Histogram of valid time spacings in  $\mathbf{O}$ . (b) Kernel-smoothed histogram of valid time spacings in  $\mathbf{O}$ .

$x_{s,i} \sim IG(\mathbf{s}_i - \mathbf{s}_{i-1}; \mu_{\text{true}}, \theta_{\text{true}})$  be the  $i$ th heartbeat inter-arrival time in  $\mathbf{S}$ . Then,

$$\mathbf{s}_m = \sum_{i=1}^m x_{s,i}, \quad \forall m \in [1, M], \quad (3)$$

where  $M$  is the total number of heartbeats in the sequence and  $\mathbf{s}_0 \triangleq 0$ . The assumption that  $\mu$  and  $\theta$  are constant is valid for a short heartbeat sequence, but in reality, both  $\mu$  and  $\theta$  can vary as functions of time.

### 2.3.2 Parameter Estimation

Given the sequence  $\mathbf{O}$  found in Section 2.2, the first task is to estimate a general  $\mu$  and  $\theta$ , given that the sequence is not long enough for the parameters to change much. The ML estimate of  $\mu$  for an  $IG$  distribution is the mean of the intervals. However, this would be a poor estimate in our case because  $\mathbf{O}$  may contain FPs and FNs. Therefore, we use a different method.

First, we find all the time intervals between subsequent heartbeats in  $\mathbf{O}$ , denoted by  $x_{o,i}$ , defined as in eq. (3). Then, we eliminate all intervals outside of the typical human range of 30-200 beats per minute (bpm):

$$\tilde{x}_{o,i} = \{x_{o,i} | 0.3\text{s} \leq x_{o,i} \leq 2\text{s}\}.$$

Next, we find the histogram of  $\tilde{\mathbf{X}}_o = \tilde{x}_{o,1}, \tilde{x}_{o,2}, \dots, \tilde{x}_{o,M}$ , and, to smooth it out, we use Gaussian kernel smoothing.<sup>20</sup> Finally, we use the inter-beat interval that corresponds to the highest value of the smoothed histogram as the value for our estimate of  $\mu$ :

$$\mu_{\text{est}} = \underset{x}{\operatorname{argmax}} \operatorname{GS}(\operatorname{Hist}(\tilde{\mathbf{X}}_o)), \quad (4)$$

where  $\operatorname{Hist}$  and  $\operatorname{GS}$  are the histogram and Gaussian smoothing operations, respectively, and the smoothed histogram is parametrized by  $x$ . Fig. 4 shows this process for an observation sequence  $\mathbf{O}$  with 65 correct locations, i.e. true positives (TPs), 35 FNs, and 15 FPs. The ML estimate of the heart rate here is 52.41 bpm, while we calculate  $\mu_{\text{est}}$  as 59.82 bpm. The true heart rate is 59.83 bpm.

The standard deviation (StD) of the  $IG$  distribution is given by  $\sqrt{\mu^3/\theta}$ . Using the value of  $\mu_{\text{est}}$  and an empirically found value of the StD of the heartbeat locations (denoted by  $\gamma$ ), we set

$$\theta_{\text{est}} = \mu_{\text{est}}^3 / \gamma^2, \quad (5)$$

where we set  $\gamma = 0.07$  s based on analyzing a large number of various ECGs.

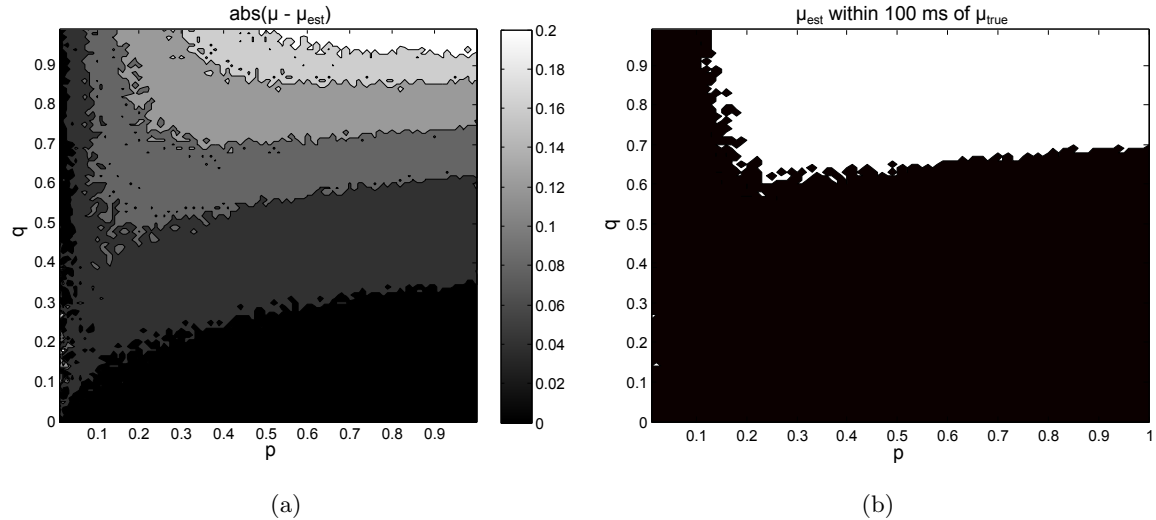


Figure 5: Region of convergence of  $\mu_{\text{est}}$  to  $\mu_{\text{true}}$ . (a) Difference between  $\mu_{\text{est}}$  and  $\mu_{\text{true}}$ . (b) The region where  $\mu_{\text{est}}$  is within 100 ms of  $\mu_{\text{true}}$  is shown in black.

In order to validate this technique, we created a model for the process of generating  $\mathbf{O}$ . The locations in  $\mathbf{O}$  are generated using an *IG* process with a given  $\mu$  and  $\theta$ . In  $\mathbf{O}$ , TPs occur with probability  $p$  (implying FNs with probability  $1 - p$ ). The number of FPs in each interval between heartbeats is determined by a geometric probability distribution with parameter  $1 - q$ . Their locations are determined by a uniform distribution over the current interval.

The parameters  $p$  and  $q$  are inherent to the detector which generates  $\mathbf{O}$ . Ideally, the detector has  $p = 1$  and  $q = 0$ . However, this is not the case in practice. Fig. 5 shows the accuracy of  $\mu_{\text{est}}$  in  $p$ - $q$  space (using the detector described in Sec. 2.2 for a sequence of 10000 heartbeats). This shows that as the number of heartbeats increases, the value of  $\mu_{\text{est}}$  approaches  $\mu_{\text{true}}$  for certain values of  $p$  and  $q$ . As long as the detector in Section 2.2 operates in a convergent region,  $\mu_{\text{est}}$  should be a good estimate for the rest of the heartbeat estimation procedure.

It should be noted, however, that not the entire convergent area is good. Towards the top left of plots in Fig. 5, there is a large number of FPs and FNs, which creates what may look like a feasible sequence of heartbeats. This may give an accurate value for  $\mu_{\text{est}}$ , but would not do well with our verification in Sec. 2.4. Therefore, it is ideal to stay as far to the bottom right in the plots of Fig. 5 as possible.

Another important note is that the FN and FP locations must be random. If they have correlation, then the procedure to find  $\mu_{\text{est}}$  will not work. For example, if every other heartbeat is missing,  $\mu_{\text{est}}$  will be  $2 \cdot \mu_{\text{true}}$ , and there is no way to recover the correct inter-beat spacings.

### 2.3.3 Modeling for Optimization

The goal of the subsequent processing will be to make a sequence  $\mathbf{Q}$  out of  $\mathbf{O}$  that is as close as possible to  $\mathbf{S}$ . A big problem is that it is very difficult to define what “as close as possible” really is. If one wants to know just the heart rate, then only the number of heartbeats in  $\mathbf{Q}$  and  $\mathbf{S}$  have to match. If one wants to minimize FPs and FNs, then the placement of the heartbeats in  $\mathbf{Q}$  should match those in  $\mathbf{S}$  as closely as possible. If one wants to analyze heart rate variability, then the relative locations of the heartbeats in  $\mathbf{Q}$  have to match those in  $\mathbf{S}$  (as opposed to absolute locations).

We start our analysis by assuming a generic model  $\mathcal{M}$  that we would like to use to minimize some cost metric  $f(\cdot)$ :

$$\mathcal{M} = \underset{\mathcal{M}}{\operatorname{argmin}} f(\mathcal{M}, \mathbf{O}). \quad (6)$$

This optimization will be broken up into two parts: pruning and interpolation (as was shown in Fig. 1). Since  $\mathbf{O}$  consists of TPs, FPs, and FNs, the goal of pruning is to eliminate the FPs in  $\mathbf{O}$  (i.e. to find a set of FPs

**P**). Then, the goal of interpolation is to eliminate the FNs in  $\mathbf{O}$  (i.e. to find a set of FNs,  $\mathbf{I}$ ). Both of these procedures will use the probabilistic model of heart rate presented in eq. (2) along with  $\mu_{\text{est}}$  and  $\theta_{\text{est}}$  found in eqs. (4) and (5). Therefore, our goal is to minimize FPs and FNs, while at the same time produce as accurate of a heart rhythm as possible. Our model is then specified by  $\mathcal{M} = \{\mathbf{P}, \mathbf{I}, IG(\tau; \mu, \theta), \mu_{\text{est}}, \theta_{\text{est}}\}$ , and our cost metric  $f(\cdot)$  is related to the probability of the resulting sequence  $\mathbf{Q}$  in the context of  $\mathbf{O}$ :

$$\mathcal{M} = \underset{\mathcal{M}}{\operatorname{argmax}} P[\mathcal{M}|\mathbf{O}], \quad (7)$$

that is, we want to maximize the probability of the model  $\mathcal{M}$  given the observation sequence  $\mathbf{O}$ .

### 2.3.4 Heartbeat Interpolation

The ideal goal of heartbeat interpolation is to fill in every FN location. If there would be no FPs in  $\mathbf{O}$  and each  $\mathbf{o}_i$  would be evenly spaced, this would entail simply finding  $\mu_{\text{est}}$  and filling in spaces much larger than  $\mu_{\text{est}}$  with the proper number of heartbeats. However, the problem is made difficult by the uneven spacing of  $\mathbf{o}_i$ s and the occurrence of FPs.

The problem can be formulated as finding the maximum a posteriori (MAP) estimate of the interpolated heartbeats as follows. Let  $\mathbf{I} = \mathbf{i}_1, \mathbf{i}_2, \dots, \mathbf{i}_L$  be a vector of interpolated heartbeats. Then, the goal is to find:

$$\hat{\mathbf{I}} = \underset{\mathbf{I}, \mu}{\operatorname{argmax}} P[\mathbf{I}, \mu|\mathbf{O}], \quad (8)$$

where  $\theta$  is uniquely determined by  $\mu$  and therefore does not factor into the optimization. This problem is general in the sense that  $\mu$  can be a function of time and is therefore optimized at the same time as  $\mathbf{I}$ . Using Bayes' Theorem, eq. (8) can be reformulated as:

$$\hat{\mathbf{I}} = \underset{\mathbf{I}, \mu}{\operatorname{argmax}} \frac{P[\mathbf{I}|\mu, \mathbf{O}]P[\mathbf{O}|\mu]P[\mu]}{P[\mathbf{O}]}, \quad (9)$$

where  $P[\mu]$  is a prior distribution on  $\mu$  and can be estimated using  $\mu_{\text{est}}$  as

$$P[\mu] \sim \mathcal{N}(\mu_{\text{est}}, \sigma^2), \quad (10)$$

where  $\mathcal{N}(a, b)$  denotes a Gaussian probability distribution with mean  $a$  and variance  $b$ , and  $\sigma$  is a standard deviation based on empirical observations of how much an individual's heart rate can change in a given period of time.

In order to solve eq. (9), we analyze  $\mathbf{O}$  in a sliding window of length  $\beta$ . Let  $\mathbf{O}_j = \mathbf{o}_j, \mathbf{o}_{j+1}, \dots, \mathbf{o}_{j+\beta-1}$  be a window of  $\beta$  observations. We then assume that the heart rate does not change for small intervals (which implies a first-order Markov property on  $\mathbf{O}$ ) and use eq. (2) to write

$$\begin{aligned} P[\mathbf{O}_j|\mu] &= \prod_{i=j+1}^{j+\beta-1} P[\mathbf{o}_i|\mathbf{o}_{i-1}, \mu] \\ &= \prod_{i=j+1}^{j+\beta-1} IG(\mathbf{o}_i - \mathbf{o}_{i-1}; \mu, \mu^3/\gamma^2). \end{aligned} \quad (11)$$

To find  $P[\mathbf{I}|\mu, \mathbf{O}]$ , we again have to make some simplifying assumptions, since a probability measure is difficult to compute when the length of the sequence  $\mathbf{I}$  can vary. We therefore assume, as before, that the heart rate does not change for short periods of time. This allows us to say that the sequence of interpolated heartbeats is equispaced in between two observations. In effect, this reduces the interpolated heartbeats to a single number,  $\pi_j$ , which is the number of interpolated heartbeats in a given interval, where  $\pi_j$  is the number of interpolated heartbeats between observations  $\mathbf{o}_{j+\lfloor\beta/2\rfloor-1}$  and  $\mathbf{o}_{j+\lfloor\beta/2\rfloor}$ . We can then write

$$\begin{aligned} P[\mathbf{I}_j|\mu, \mathbf{O}_j] &= P[\pi_j|\mu, \mathbf{O}_j] \\ &= IG\left(\frac{\mathbf{o}_{j+\lfloor\beta/2\rfloor-1} - \mathbf{o}_{j+\lfloor\beta/2\rfloor}}{\pi_j + 1}; \mu, \mu^3/\gamma^2\right). \end{aligned} \quad (12)$$

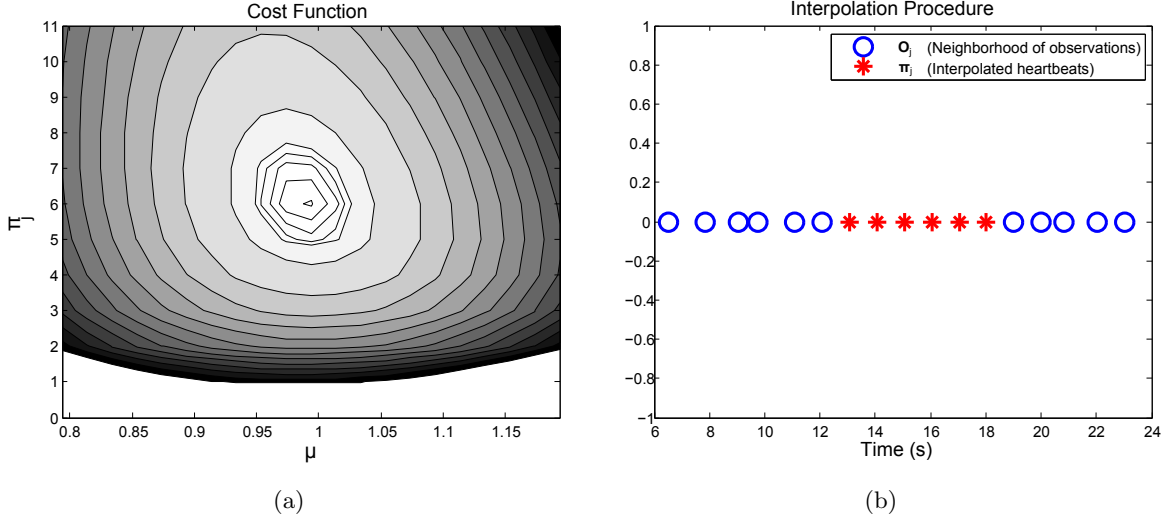


Figure 6: Heartbeat interpolation sample procedure. (a) Cost function (eq. (13)) of a neighborhood  $j$ . (b) Interpolated heartbeats ( $\pi_j^*$ ).

Using eqs. (10), (11), and (12), we can solve eq. (9) in a sliding window:

$$\pi_j^* = \underset{\pi_j, \mu}{\operatorname{argmax}} P[\pi_j | \mu, \mathbf{O}_j] P[\mathbf{O}_j | \mu] P[\mu], \quad (13)$$

where we have discarded  $P[\mathbf{O}]$  in the denominator of eq. (9) since it is not a function of  $\pi_j$  or  $\mu$ . An example of this procedure can be seen in Fig. 6. Combining all the interpolated heartbeats into  $\hat{\mathbf{I}} = \{\pi_j^*\}$ , we get the interpolated sequence  $\mathbf{O}_I$  as

$$\mathbf{O}_I = \{\mathbf{O}\} \cup \{\hat{\mathbf{I}}\} \quad (14)$$

### 2.3.5 Heartbeat Pruning

Given a set of heartbeat temporal locations,  $\mathbf{O}$ , the goal of pruning is to eliminate heartbeats which do not belong from a probabilistic viewpoint:

$$\hat{\mathbf{P}} = \underset{\mathbf{P}, \mu}{\operatorname{argmax}} P[\mathbf{P}, \mu | \mathbf{O}], \quad (15)$$

where  $\mu$ , the mean of the inverse Gaussian governing process, is considered part of the optimization as well because it can vary locally. The maximum a posteriori (MAP) estimate of  $\mathbf{P}$  can be formulated as

$$\hat{\mathbf{P}} = \underset{\mathbf{P}, \mu}{\operatorname{argmax}} \frac{P[\mathbf{O} | \mathbf{P}, \mu] P[\mathbf{P}, \mu]}{P[\mathbf{O}]}. \quad (16)$$

The probability measure  $P[\mathbf{O} | \mathbf{P}, \mu]$  is intractable, since it is a combinatorial problem (where  $\mathbf{P}$  can be any subset of  $\mathbf{O}$ ). In addition,  $P[\mathbf{P}, \mu]$  is poorly defined. Therefore, we must reformulate the problem to make it solvable.

Instead of finding a subset of  $\mathbf{O}$  directly, we find the probability that each element of  $\mathbf{O}$  is not a FP. This analysis is performed using a sliding window of length  $\alpha$ . Let  $\mathbf{O}_j = \mathbf{o}_j, \mathbf{o}_{j+1}, \dots, \mathbf{o}_{j+\alpha-1}$  be a window of  $\alpha$  observations. Then,

$$\{\hat{\mathbf{I}}_{P,j}, \mu_j^*\} = \underset{\mathbf{I}_{P,j}, \mu}{\operatorname{argmax}} \frac{P[\mathbf{I}_{P,j} | \mu, \mathbf{O}] P[\mathbf{O} | \mu] P[\mu]}{P[\mathbf{O}]}, \quad (17)$$

where  $\mathbf{I}_{P,j}$  is a sequence of interpolated heartbeats in the  $j$ th window (composed of  $\pi_{P,j}$  equispaced heartbeats

as in Sec. 2.3.4, where  $\pi_{P,j}^*$  corresponds to  $\hat{\mathbf{I}}_{P,j}$  as before), obtained using

$$\begin{aligned} P[\mathbf{O}_j|\mu] &= \prod_{i=j+1}^{j+\alpha-1} P[\mathbf{o}_i|\mathbf{o}_{i-1}, \mu] \\ &= \prod_{i=j+1}^{j+\alpha-1} IG(\mathbf{o}_i - \mathbf{o}_{i-1}; \mu, \mu^3/\gamma^2) \end{aligned} \quad (18)$$

$$P[\mu] \sim \mathcal{N}(\mu_{\text{est}}, \sigma^2) \quad (19)$$

$$\begin{aligned} P[\mathbf{I}_{P,j}|\mu, \mathbf{O}_j] &= P[\pi_{P,j}|\mu, \mathbf{O}_j] \\ &= IG\left(\frac{\mathbf{O}_{j+\alpha-1} - \mathbf{O}_j}{\pi_{P,j} + 1}; \mu, \mu^3/\gamma^2\right), \end{aligned} \quad (20)$$

which is akin to eqs. (9), (10), (11), and (12), where we now use the outermost heartbeats in  $\mathbf{O}_j$  as opposed to the center ones for interpolation.

Then, we want to find the probability that the individual heartbeats in  $\mathbf{O}_j$  conform to the modeled heartbeats  $\hat{\mathbf{I}}_{P,j}$ , and that  $\hat{\mathbf{I}}_{P,j}$  is a good model for the interval:

$$\begin{aligned} c_{j,k} &= P[\mathbf{o}_{j+k-1}, \mathbf{I}_{P,j} = \hat{\mathbf{I}}_{P,j}, \mu = \mu_j^*], & \forall k \in [2, \alpha - 1] \\ &= P[\mathbf{o}_{j+k-1}|\mathbf{I}_{P,j} = \hat{\mathbf{I}}_{P,j}, \mu = \mu_j^*] \cdot P[\mathbf{I}_{P,j} = \hat{\mathbf{I}}_{P,j}|\mu = \mu_j^*] \cdot P[\mu = \mu_j^*], & \forall k \in [2, \alpha - 1] \\ &= \mathcal{N}(\mathbf{o}_{j+k-1}; \hat{\mathbf{i}}_{P,j,k}, \sigma^2) \cdot IG\left(\frac{\mathbf{O}_{j+\alpha-1} - \mathbf{O}_j}{\pi_{P,j}^* + 1}; \mu_j^*, (\mu_j^*)^3/\gamma^2\right) \cdot \mathcal{N}(\mu_j^*; \mu_{\text{est}}, \sigma^2), & \forall k \in [2, \alpha - 1], \end{aligned} \quad (21)$$

where  $\hat{\mathbf{i}}_{P,j,k}$  is the element of  $\hat{\mathbf{I}}_{P,j}$  closest to  $\mathbf{o}_{j+k-1}$  and  $\sigma$  is the same as used previously. Adding together all the  $c_{j,k}$  elements that correspond to each  $\mathbf{o}_i$  forms the sequence  $\mathbf{C} = \{\mathbf{c}_i\}$ , which is the confidence in each observation in  $\mathbf{O}$ .

The pruned heartbeats  $\hat{\mathbf{P}}$  are then found as

$$\hat{\mathbf{P}} = \{\mathbf{o}_i | \mathbf{c}_i < (\mu_C - 0.5\sigma_C)\} \quad \forall i \in [1, N], \quad (22)$$

where

$$\mu_C = \frac{1}{N} \sum_{i=1}^N \mathbf{c}_i, \quad \sigma_C = \left( \frac{1}{N-1} \sum_{i=1}^N (\mathbf{c}_i - \mu_C)^2 \right)^{\frac{1}{2}}.$$

The pruning procedure can be seen in Fig. 7. Once we find the pruned heartbeats  $\hat{\mathbf{P}}$ , we can form the sequence  $\mathbf{O}_P$  as

$$\mathbf{O}_P = \{\mathbf{O}\} \setminus \{\hat{\mathbf{P}}\}, \quad (23)$$

which is the sequence  $\mathbf{O}$  with the pruned heartbeats  $\hat{\mathbf{P}}$  removed.

### 2.3.6 Heartbeat Estimation and Validation

After obtaining  $\mathbf{O}$  as described in Sec. 2.2, pruning is performed to get  $\mathbf{O}_P$  according to eqs. (15) and (23). Then,  $\mathbf{O}_P$  is used as the input to the interpolation procedure to get  $\mathbf{O}_I$  according to eqs. (9) and (14). After this,  $\mathbf{O}_I$  is used as the input to the pruning procedure, and so on, until  $\hat{\mathbf{P}} = \hat{\mathbf{I}} = \emptyset$ , as shown in Fig. 1. At this point, we set  $\mathbf{Q} = \mathbf{O}_I$ , where  $\mathbf{Q} = \mathbf{q}_1, \mathbf{q}_2, \dots, \mathbf{q}_D$ .

The final step of the heartbeat estimation procedure is to make sure that  $\mathbf{Q}$  is a valid heartbeat sequence, i.e. the intervals in  $\mathbf{Q}$  make physiological sense. We set the upper bound of heart rate to 200 bpm, and sweep across  $\mathbf{Q}$ , checking each interval  $(\mathbf{q}_{i+1} - \mathbf{q}_i, i \in \{2, 3, \dots, D-2\})$ . If the interval is too short, then we use

$$P_i = IG(\mathbf{q}_i - \mathbf{q}_{i-1}; \mu_{\text{est}}, \theta_{\text{est}}) \cdot IG(\mathbf{q}_{i+2} - \mathbf{q}_i; \mu_{\text{est}}, \theta_{\text{est}}), \quad (24)$$

$$P_{i+1} = IG(\mathbf{q}_{i+1} - \mathbf{q}_{i-1}; \mu_{\text{est}}, \theta_{\text{est}}) \cdot IG(\mathbf{q}_{i+2} - \mathbf{q}_{i+1}; \mu_{\text{est}}, \theta_{\text{est}}). \quad (25)$$

Eq. (24) is the probability that the  $i$ th heartbeat fits into the overall process, and eq. (25) is the probability that the  $(i+1)$ st heartbeat fits into the overall process. If  $P_i > P_{i+1}$ , then we eliminate  $\mathbf{q}_{i+1}$ ; if  $P_i < P_{i+1}$ , then we eliminate  $\mathbf{q}_i$ . This guarantees that  $\mathbf{Q}$  is a feasible physiological process.

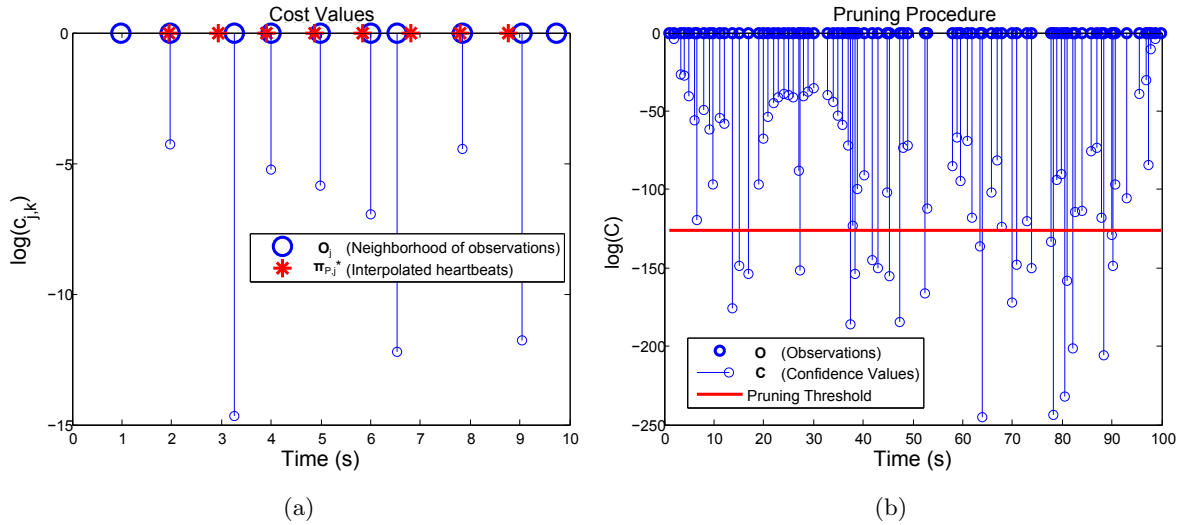


Figure 7: Heartbeat pruning sample procedure. (a) Cost function (eq. (21)) of a neighborhood  $\mathbf{o}_j$ . (b) Observation sequence  $\mathbf{O}$  with associated confidence values  $\mathbf{C}$ .

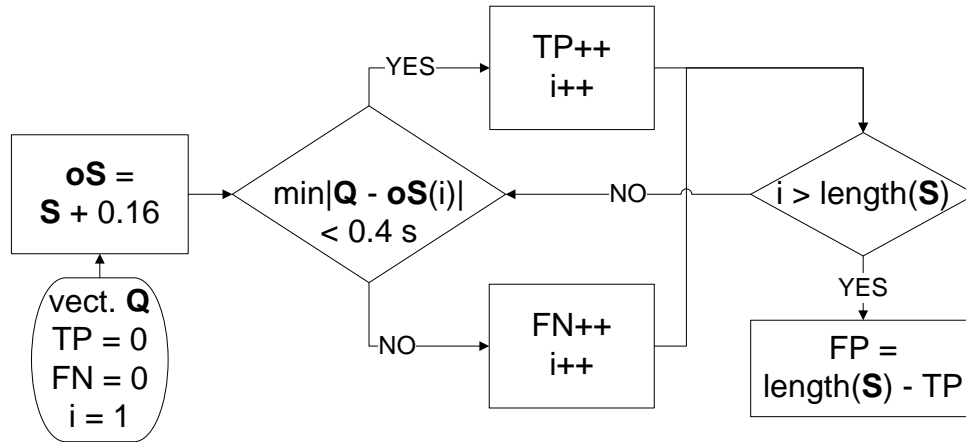


Figure 8: Flowchart of verification algorithm.

## 2.4 Result Verification

In order to consistently evaluate the performance of the algorithm, we created a verification algorithm. First, we find the peaks of the QRS complexes in the concurrently-gathered ECG using the Pan-Tompkins algorithm,<sup>21</sup> which creates the sequence  $\mathbf{S}$ . Then, each value in  $\mathbf{S}$  is offset by 0.16 s, an empirically-determined value to account for the time between the QRS-complex and the propagation of the heart motion to the chest wall ( $\mathbf{oS}$  in Fig. 8). Next, each value in  $\mathbf{Q}$  is compared to  $\mathbf{oS}$ . If a heartbeat falls within 0.4 s of an element of  $\mathbf{oS}$ , it is counted as a true positive (TP); otherwise, it is counted as a false positive (FP). If there is no element of  $\mathbf{Q}$  within 0.4 s of any element of  $\mathbf{oS}$ , it is counted as a false negative (FN). True negatives (TN) do not apply to this data, as we are only interested in finding the presence of heartbeats, not their absence. The whole process can be seen in the flowchart in Fig. 8.

Using these measures, we are able to find the recall (or sensitivity) and precision as

$$\text{Recall} = \frac{\text{TP}}{\text{TP} + \text{FN}} \quad (26)$$

$$\text{Precision} = \frac{\text{TP}}{\text{TP} + \text{FP}} \quad (27)$$

These measures are a good indication as to the accuracy of the algorithm, as they take not only the heart rate

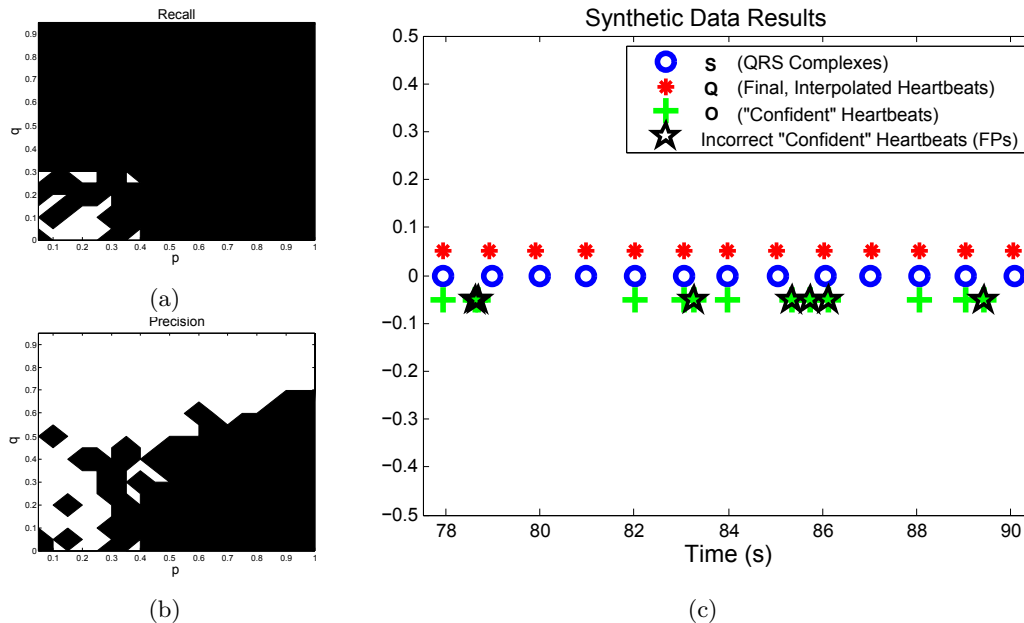


Figure 9: Results of applying our algorithm on synthetic data for varying  $p$  and  $q$ . (a) Recall - black area indicates recall  $> 98\%$ . (b) Precision - black area indicates precision  $> 98\%$ . (c) Sample sequence showing **S**, **Q**, **O**, and FP locations, when  $p=0.6$  and  $q=0.3$ .

into account, but also the actual heartbeat temporal locations. If we were to simply use the average of the inter-beat spacings to calculate the heart rate, a large number of false positives followed by a large number of false negatives might give an accurate heart rate. However, using this verification algorithm, only accurately placed heartbeats contribute to the true positive count.

### 3. RESULTS

In this section, we present the results of using the algorithm described in Sec. 2 in several scenarios, ranging from simplest to most complicated. For all of our tests, we used  $\alpha = 10$  (Sec. 2.3.5) and  $\beta = 11$  (Sec. 2.3.4), based on cross validation.

#### 3.1 Synthetic Data

##### 3.1.1 Generated Data

The first test of our algorithm was to use it on data generated using the model presented in Sec. 2.3.2 with varying  $p$  and  $q$  to simulate various ratios of FNs and FPs. We used a  $\mu_{\text{true}}$  value of 1.0 s to simulate a heart rate of 60 bpm. The shape parameter  $\theta_{\text{true}}$  was set to  $\mu_{\text{true}}^3/\gamma^2 = 204.08$  s in order to keep a standard deviation of 0.07 s as was established in Sec. 2.3.2. The results of using our algorithm with various  $p$  and  $q$  values are presented in Fig. 9, along with a sample sequence in Fig. 9(c), with  $p=0.6$  and  $q=0.3$ .

##### 3.1.2 ECG Data

The next test of our algorithm was done using ECG samples from the Physionet<sup>22</sup> databases. Here, we used actual patients' ECG data, but removed and added heartbeats in the same way as before by varying  $p$  and  $q$ . Once again, the results of our algorithm for a given dataset are presented in Fig. 10, with an example sequence shown in Fig. 10(c) with  $p=0.6$  and  $q=0.3$ .

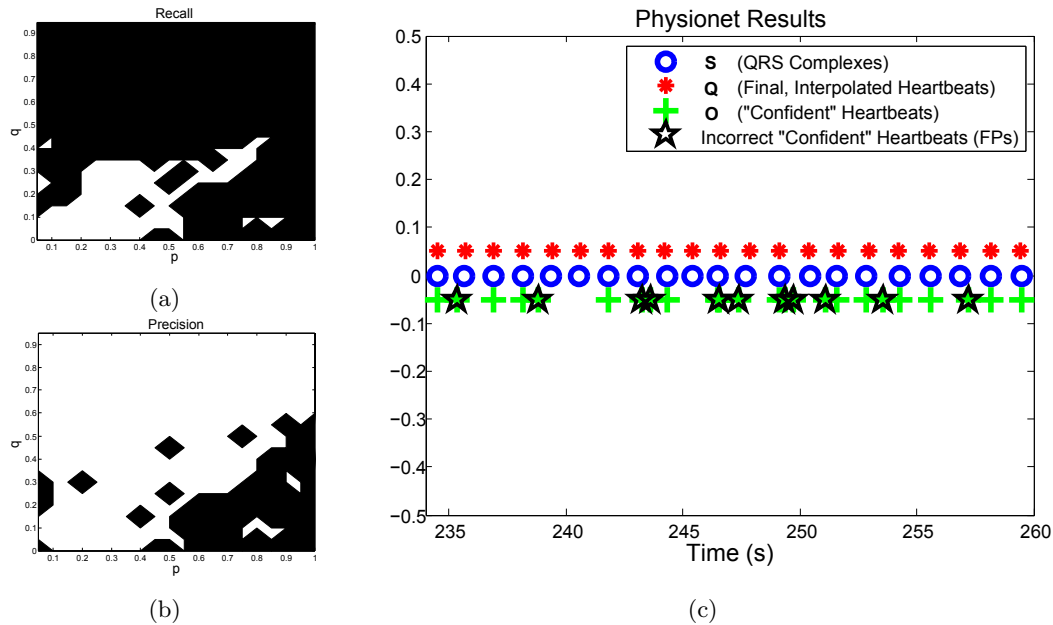


Figure 10: Results of applying our algorithm on Physionet data for varying  $p$  and  $q$ . (a) Recall - black area indicates recall > 98%. (b) Precision - black area indicates precision > 98%. (c) Sample sequence showing S, Q, O, and FP locations, when  $p=0.6$  and  $q=0.3$ .

Table 1: Description of Subjects.

Subject #	Gender	Age	Height (cm)	BMI
1	F	20	164	18.3
2	M	24	180	26.5
3	M	25	173	22.8
4	M	26	168	20.2
5	M	57	173	25.5

### 3.2 Millimeter-wave Data

The most important validation of our algorithm was on actual data captured by our millimeter-wave system (Sec. 2.1). For these tests, we received approval from Northwestern University's Office for the Protection of Research Subjects (IRB Project Number: STU00051704).

We tested our algorithm on data from stationary subjects as well as mobile ones. The displacement of the chest wall due to cardiac activity is on the order of  $10^{-4}$  m, while that due to respiration varies from approximately 0.004 to 0.012 m.<sup>23</sup> The movement that we processed was more than 1 m, which is several orders of magnitude greater than that due to cardiac activity.

For our tests, we had five subjects. Their characteristics are presented in Table 1. They all followed the same test protocol, described as follows. Starting out seated 3.5 m from the sensor for about 15 s, the subject then stood up and walked slowly toward the sensor until 2 m away. After that, the subject moved backward until 4 m from the sensor, and remained at that distance for about 40 s. Finally, the subject walked more quickly to a distance of 2 m from the sensor.

The results can be seen in Table 2, where  $|S|$  is the total number of actual heartbeats (in the ECG) and the state designation  $m$  means the subject was moving, while  $nm$  means the subject was not moving. A sample sequence for data with movement is presented in Fig. 11.

Table 2: Results of Proposed Algorithm.

State	S	TP	FP	FN	Rec	Prec
m	777	728	47	49	93.7%	93.9%
nm	1469	1362	103	107	92.7%	93.0%
N/A	2246	2090	150	156	<b>93.1%</b>	<b>93.3%</b>

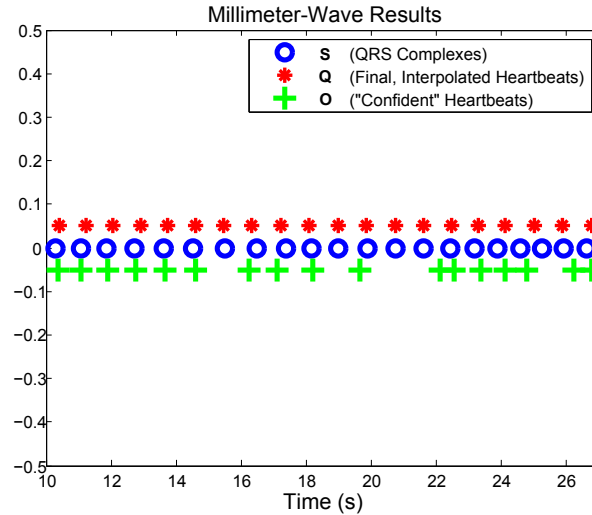


Figure 11: Results of applying our algorithm on millimeter-wave data.

#### 4. DISCUSSION

When used on synthetic data, our algorithm performs very well, even in the presence of significantly many FNs and FPs. It is important to note, however, that the standard deviations of the inter-beat times in data in Sec. 3.1.1 were set to be similar to real-life ECGs, and Sec. 3.1.2 used real ECGs. The standard deviation of the inter-beat times created by the algorithm in Sec. 2.2, in relation to the concurrently-gathered ECG, were approximately five times larger than those in the ground truth. This extra variability made the probabilistic pruning and adding much more difficult, since these algorithms rely on the confidence that a series of heartbeat locations “looks” correct. Therefore, the algorithm could potentially perform much better if the processing to determine **O** is improved.

A big advantage of this algorithm is that it uses the inherent statistics of the observations **O** without relying on heuristics and training, as was done in our previous work.<sup>14</sup> Here, there is no need to train on data to adjust thresholds (except for the pruning in eq. (22)), since everything is formulated in a Bayesian inference framework. Even so, the results are better on data with movement than with the previous algorithm.

The detector that was used in this work (Sec. 2.2) performed with  $p = 0.793$  and  $q = 0.065$ . This put us well within the convergent region in Fig. 5, which means that our estimate of  $\mu_{\text{est}}$  and  $\theta_{\text{est}}$  should be correct, given a long enough sequence of observations. However, since the real observation sequences were not very long, our pruning and interpolation algorithms had a harder time with some sequences.

The threshold in eq. (22), i.e.  $(\mu_C - 0.5\sigma_C)$ , can be tuned for different types of detectors. The smaller it is, the more aggressive the pruning will be. This would be useful if the detector admits a large number of FPs, in which case it would be advantageous to eliminate more observations, even though more TPs would be pruned as well. This would then rely more heavily on the interpolation procedure to fill in the FN locations. In this scenario, it would be important to have a very small deviation of the correct observations from the true heartbeat locations, because any deviation would be exacerbated by the interpolation procedure. On the other hand, using a high threshold would result in more modest pruning. We chose the value we did because it created a good mix of the two pruning regimes for our detector, and created an even mix of FPs and FNs as is shown in Table 2.

Table 3: Run Time of Algorithm Components.

	Find $\mathbf{O}$	Prune	Interpolate	Validate	<b>Total</b>
Time (s)	0.1865	0.0060	0.0131	0.0011	0.4007

One aspect of our validation on synthetic data in Sec. 3.1 that stood out was that the recall tended to be higher than the precision. This implies a larger number of FPs as compared to FNs. This, however, was not the case when testing on real data in Sec. 3.2. We think this is because our algorithm for creating FPs in the synthetic cases is potentially too harsh. As can be seen in Fig. 10(c), the FP locations can be in very difficult locations despite a modest value of  $q$ . This of course gets even worse for larger values of  $q$ . The FP locations in the real data were not so clustered as in the synthetic data. However, this more challenging scenario was a good test of our algorithm, and we still got very good results.

It should be noted that the proposed algorithm works properly only for regular cardiac rhythms. For subjects exhibiting intermittent long inter-beat intervals, this method would interpolate heartbeats in the large intervals and create a healthy-looking output. Also, some subjects, such as young people, might have a heart rate faster than 200 bpm, in which case the algorithm would prune heartbeats in order to enforce a rate under 200 bpm. However, although this algorithm may not be ready for medical diagnostics, it would perform well in a security setting where the important characteristic is the subject's average heart rate.

An important aspect in a security setting is how quickly the algorithm could detect a change in heart rate, as this is a potential marker for suspicious activity. Since our algorithm operates in a local window, an entirely new set of statistics would be obtained every  $\max(\alpha, \beta)$  heartbeats, or 11 heartbeats for our settings. This means that a sudden change in heart rate would be detected in  $\sim 10$  s.

As far as the speed of the algorithm, it could potentially be implemented in near-real time. It was used here strictly for post-processing on longer signals. However, if we first use a larger window to get  $\mu_{\text{est}}$ , we can then operate on a moving window of size  $\max(\alpha, \beta)$ , which is 11 heartbeats in our case. While we have not implemented this version of the algorithm, we have measured the run-times of the various components over 100 iterations, presented in Table 3. As can be seen, the entire algorithm can run in  $\sim 0.4$ s on 11 heartbeats, making near-real time implementation a possibility. All measurements were made using a Windows 7 64-bit machine with an Intel W3580 CPU with 12 GB of RAM.

## 5. CONCLUSION

The proposed probabilistic algorithm represents an improvement over our previous method<sup>14</sup> because it uses a solid Bayesian inference framework as opposed to statistical heuristics to find missing heartbeats and to prune incorrect observations. The ability to accommodate for local variations in heart rate, due to effects such as respiratory sinus arrhythmia, is also a big advantage of this method. However, heartbeat temporal irregularities are impossible to interpolate correctly if there are large intervals with no observations. Therefore, it is important that we have developed a good algorithm for generating  $\mathbf{O}$  before we begin our post-processing.

It should be noted, very importantly, that we have presented an algorithm that works on moving subjects in realistic scenarios. To the authors' knowledge, this has only been reported once before,<sup>14</sup> and the proposed algorithm has outperformed that one. Future work will focus on better techniques in Sec. 2.2, since the better the initial locations in  $\mathbf{O}$  become, the better our algorithm will perform.

## REFERENCES

- [1] Uenoyama, M., Matsui, T., Yamada, K., Suzuki, S., Takase, B., Suzuki, S., Ishihara, M., and Kawakami, M., "Non-contact respiratory monitoring system using a ceiling-attached microwave antenna," *Medical and Biological Engineering and Computing* **44**(9), 835–840 (2006).
- [2] Bakhtiari, S., Elmer, T. W., Cox, N. M., Gopalsami, N., Raptis, A. C., Liao, S., Mikhelson, I., and Sahakian, A. V., "Compact millimeter-wave sensor for remote monitoring of vital signs," *Instrumentation and Measurement, IEEE Transactions on* **61**, 830–841 (march 2012).

- [3] Geisheimer, J. and Greneker III, E. F., "A non-contact lie detector using radar vital signs monitor (RVSM) technology," *Aerospace and Electronic Systems Magazine, IEEE* **16**(8), 10–14 (2001).
- [4] Lubecke, V. M., Boric-Lubecke, O., Host-Madsen, A., and Fathy, A. E., "Through-the-wall radar life detection and monitoring," in [*Microwave Symposium, 2007. IEEE/MTT-S International*], 769–772, IEEE (2007).
- [5] Chekmenev, S. Y., Rara, H., and Farag, A. A., "Non-contact, wavelet-based measurement of vital signs using thermal imaging," in [*The first international conference on graphics, vision, and image processing (GVIP), Cairo, Egypt*], 107–112 (2005).
- [6] Zalevsky, Z., Beiderman, Y., Margalit, I., Gingold, S., Teicher, M., Mico, V., and Garcia, J., "Simultaneous remote extraction of multiple speech sources and heart beats from secondary speckles pattern," *Optics Express* **17**(24), 21566–21580 (2009).
- [7] Poh, M.-Z., McDuff, D. J., and Picard, R. W., "Non-contact, automated cardiac pulse measurements using video imaging and blind source separation," *Optics Express* **18**(10), 10762–10774 (2010).
- [8] Lin, J. C., "Microwave sensing of physiological movement and volume change: A review," *Bioelectromagnetics* **13**(6), 557–565 (1992).
- [9] Morgan, D. R. and Zierdt, M. G., "Novel signal processing techniques for doppler radar cardiopulmonary sensing," *Signal Processing* **89**(1), 45–66 (2009).
- [10] Obeid, D., Sadek, S., Zaharia, G., and Zein, G. E., "Noncontact heartbeat detection at 2.4, 5.8, and 60 GHz: A comparative study," *Microwave and Optical Technology Letters* **51**(3), 666–669 (2009).
- [11] Petkie, D. T., Benton, C., and Bryan, E., "Millimeter wave radar for remote measurement of vital signs," in [*Radar Conference, 2009 IEEE*], 1–3, IEEE (2009).
- [12] Mikhelson, I. V., Bakhtiari, S., Elmer, II, T. W., and Sahakian, A. V., "Remote sensing of heart rate and patterns of respiration on a stationary subject using 94-GHz millimeter-wave interferometry," *Biomedical Engineering, IEEE Transactions on* **58**, 1671–1677 (June 2011). DOI:10.1109/TBME.2011.2111371.
- [13] Lubecke, O. B., Ong, P. W., and Lubecke, V. M., "10 GHz Doppler radar sensing of respiration and heart movement," in [*Bioengineering Conference, 2002. Proceedings of the IEEE 28th Annual Northeast*], 55–56, IEEE (2002).
- [14] Mikhelson, I. V., Bakhtiari, S., Elmer II, T. W., and Sahakian, A. V., "Remote sensing of patterns of cardiac activity on an ambulatory subject using millimeter-wave interferometry and statistical methods," *Medical & biological engineering & computing* **51**(1-2), 135–142 (2013).
- [15] Jianqi, W., Chongxun, Z., Guohua, L., and Xijing, J., "A new method for identifying the life parameters via radar," *EURASIP Journal on Applied Signal Processing* **2007**(1), 16–16 (2007).
- [16] Mikhelson, I., Lee, P., Bakhtiari, S., Elmer, T., Katsaggelos, A., and Sahakian, A., "Non-contact millimeter-wave real-time detection and tracking of heart rate on an ambulatory subject," *Transactions on Information Technology in Biomedicine* **16**(5), 927–934 (2012).
- [17] Rioul, O. and Vetterli, M., "Wavelets and signal processing," *Signal Processing Magazine, IEEE* **8**(4), 14–38 (1991).
- [18] MATLAB, [*version 7.10.0 (R2010a)*], The MathWorks Inc., Natick, Massachusetts (2010).
- [19] Barbieri, R., Matten, E., Alabi, A., and Brown, E., "A point-process model of human heartbeat intervals: new definitions of heart rate and heart rate variability," *American Journal of Physiology-Heart and Circulatory Physiology* **288**(1), H424–H435 (2005).
- [20] Bowman, A. W. and Azzalini, A., "Applied smoothing techniques for data analysis," (1997).
- [21] Pan, J. and Tompkins, W. J., "A real-time QRS detection algorithm," *Biomedical Engineering, IEEE Transactions on* **BME-32**(3), 230–236 (1985).
- [22] Goldberger, A. L., Amaral, L. A. N., Glass, L., Hausdorff, J. M., Ivanov, P. C., Mark, R. G., Mietus, J. E., Moody, G. B., Peng, C.-K., and Stanley, H. E., "PhysioBank, PhysioToolkit, and PhysioNet: Components of a new research resource for complex physiologic signals," *Circulation* **101**(23), e215–e220 (2000 (June 13)). Circulation Electronic Pages: <http://circ.ahajournals.org/cgi/content/full/101/23/e215> PMID:1085218; doi: 10.1161/01.CIR.101.23.e215.
- [23] Droitcour, A. D., *Non-contact measurement of heart and respiration rates with a single-chip microwave doppler radar*, PhD thesis, Stanford University (2006).